Research Article | Vol. 24, No. 16 | 8 Aug 2016 | OPTICS EXPRESS 17644

Optics EXPRESS

Large area compatible broadband superabsorber surfaces in the VIS-NIR spectrum utilizing metal-insulator-metal stack and plasmonic nanoparticles

SINA ABEDINI DERESHGI,[1,2] AND ALI KEMAL OKYAY[1,2,3,*]

[1]*Department of Electrical and Electronics Engineering, Bilkent University, Ankara 06800, Turkey*
[2]*UNAM-National Nanotechnology Research Center, Bilkent University, Ankara 06800, Turkey*
[3]*Institute of Material Science and Nanotechnology, Bilkent University, Ankara 06800, Turkey*
[*]*aokyay@ee.bilkent.edu.tr*

Abstract: Plasmonically enhanced absorbing structures have been emerging as strong candidates for photovoltaic (PV) devices. We investigate metal-insulator-metal (MIM) structures that are suitable for tuning spectral absorption properties by modifying layer thicknesses. We have utilized gold and silver nanoparticles to form the top metal (M) region, obtained by dewetting process compatible with large area processes. For the middle (I) and bottom (M) layers, different dielectric materials and metals are investigated. Optimum MIM designs are discussed. We experimentally demonstrate less than 10 percent reflection for most of the visible (VIS) and near infrared (NIR) spectrum. In such stacks, computational analysis shows that the bottom metal is responsible for large portion of absorption with a peak of 80 percent at 1000 nm wavelength for chromium case.

OCIS codes: (040.5160) Photodetectors; (040.5350) Photovoltaic; (250.0250) Optoelectronics.

References and links

1. K. Aydin, V. E. Ferry, R. M. Briggs, and H. A. Atwater, "Broadband polarization-independent resonant light absorption using ultrathin plasmonic super absorbers," Nat. Commun. **2**, 517 (2011).
2. W. Kim, B. S. Simpkins, J. P. Long, B. Zhang, J. Hendrickson, and J. Guo, "Localized and nonlocalized plasmon resonance enhanced light absorption in metal-insulator-metal nanostructures," J. Opt. Soc. Am. B **32**(8), 1686–1692 (2015).
3. K. Islam, A. Alnuaimi, E. Battal, A. K. Okyay, and A. Nayfeh, "Effect of gold nanoparticles size on light scattering for thin film amorphous-silicon solar cells," Sol. Energy **103**, 263–268 (2014).
4. Z. M. Saleh, H. Nasser, E. Özkol, M. Günöven, K. Abak, S. Canli, A. Bek, and R. Turan, "Optimized spacer layer thickness for plasmonic-induced enhancement of photocurrent in a-Si:H," J. Nanopart. Res. **17**(10), 419 (2015).
5. S. H. Lim, W. Mar, P. Matheu, D. Derkacs, and E. T. Yu, "Photocurrent spectroscopy of optical absorption enhancement in silicon photodiodes via scattering from surface plasmon polaritons in gold nanoparticles," J. Appl. Phys. **101**(10), 104309 (2007).
6. F. Wang and N. A. Melosh, "Plasmonic energy collection through hot carrier extraction," Nano Lett. **11**(12), 5426–5430 (2011).
7. R. J. Peláez, T. Kuhn, C. E. Rodríguez, and C. N. Afonso, "Dynamics of laser induced metal nanoparticle and pattern formation," Appl. Phys. Lett. **106**(6), 061914 (2015).
8. M. C. Günendi, İ. Tanyeli, G. B. Akgüç, A. Bek, R. Turan, and O. Gülseren, "Understanding the plasmonic properties of dewetting formed Ag nanoparticles for large area solar cell applications," Opt. Express **21**(15), 18344–18353 (2013).
9. M. W. Knight, H. Sobhani, P. Nordlander, and N. J. Halas, "Photodetection with active optical antennas," Science **332**(6030), 702–704 (2011).
10. M. A. Nazirzadeh, F. B. Atar, B. B. Turgut, and A. K. Okyay, "Random sized plasmonic nanoantennas on Silicon for low-cost broad-band near-infrared photodetection," Sci. Rep. **4**, 7103 (2014).
11. F. B. Atar, E. Battal, L. E. Aygun, B. Daglar, M. Bayindir, and A. K. Okyay, "Plasmonically enhanced hot electron based photovoltaic device," Opt. Express **21**(6), 7196–7201 (2013).
12. L. Legert and J. F. Joanny, "Liquid spreading," Rep. Prog. Phys. **55**(4), 431–486 (1992).
13. E. Palik, *Handbook of Optical Constants of Solids* (Academic, 1985).
14. P. B. Johnson and R. W. Christy, "Optical constants of the noble metals," Phys. Rev. B **6**(12), 4370–4379 (1972).

#268177 http://dx.doi.org/10.1364/OE.24.017644
Journal © 2016 Received 14 Jun 2016; revised 15 Jul 2016; accepted 20 Jul 2016; published 25 Jul 2016

Optics EXPRESS

1. Introduction

As optoelectronic devices keep scaling down interminably, hot electron based plasmonic structures have been considered as promising candidates in providing low cost ultra-thin PV devices in last decades. Since plasmonic structures are highly geometry dependent, we can customize them as active absorbing layers in solar cells and photodetectors to manipulate their absorption bands and peaks in wavelength spectrum by tuning their geometry. In recent years a lot of effort has been devoted to utilize and improve plasmonic active layers. Aydin *et al.* reported broadband MIM absorbing stack with electron beam (e-beam) lithography method which reaches to an average absorption of 71 percent within 400 nm to 700 nm wavelength range [1]. Kim *et al.* put forth MIM absorbing stacks while focusing on identifying the bases of localized and non-localized plasmon resonance enhanced absorptions [2]. A set of studies on PV devices are available utilizing random nanoparticles for enhanced plasmonic absorption for solar cells and photodiodes [3–5], while Wang *et al.* propose an MIM stack carrying the burden of both absorption and photocurrent generation which would place harsh restrictions on device engineering to comply with desirable electrical and photonic characteristics [6]. There has been numerous efforts to attain random nanoparticles by laser-induced and heat-induced dewetting [7,8].

In this work we focus mainly on absorbing MIM structure and engineer broadband absorbers with low cost methods that can enjoy a seamless transition to wide areas and curved surfaces. We propose and survey dewetting of thin continuous gold and silver layers to form random nanoislands. The main advantages of dewetting are its low cost, easy fabrication and broader absorption spectrum compared to other traditional but expensive methods like e-beam lithography and focused ion beam writing. The most prominent advantages, however, are the capability of applying them to vast area and curved surfaces easily as well as polarization independency of the particles for the incoming light. The drawback on the other hand, is assuring that a substrate that can withstand high processing temperatures is used. In addition, there is a trade-off between the absorptivity and the broadening of the absorption spectrum. The latter issue builds up the backbone of the criterion for choosing the most optimum design.

Random nanoparticles can be tuned for photodetector structures, where the light excites localized surface plasmons (LSP) or surface plasmons (SP) and their non-radiative decay results in energetic hot electron-hole pairs which can be harnessed as photocurrent for photodetector applications [9,10]. Once a good absorber is designed, the MIM structure can be integrated on top of a separate hot electron or hole collecting structure to form a highly efficient metal-insulator-metal-insulator-metal (MIMIM) PV device. The light would excite SPs and the non-radiative decay would again generate energetic electron-hole pairs for photocurrent [11]. The obvious and prominent advantage of MIMIM devices is the possibility of tuning electrical and optical stacks separately which brings forward high flexibility of engineering each to achieve most optimum functionality.

2. Experimental results

2.1 Dewetting

In some metals like gold and silver, when deposited thin enough, the metal-air interfaces will not be stable. If the film is in the order of a few nanometers, not only is the deposited film unstable but also it can barely be regarded as a continuous film. If the thickness increases to the order of 10nm, the film is in thermodynamically metastable state meaning that under some excitation, the film will agglomerate in islands to minimize the vicinity with air with a specific contact angle [12]. Dewetting highly depends on the surface under the metal, the metal type and annealing process parameters. Our target design inferred that in order to attain absorption in VIS-NIR, the nanoparticle sizes must be approximately 100nm. A set of trials inferred that 10nm deposition by thermal evaporation at a pressure of 3-5 $\times$ 10^{-6} Torr is reasonable. The excitation for dewetting is applied using Eurotherm rapid thermal annealing system in 120 sccm N_2 flow rate. Figures 1(a)-1(f) are the SEM images illustrating dewetting

Optics EXPRESS

behavior of thin gold and silver films on aluminum oxide layers with respect to the applied rise and fall time of heating.

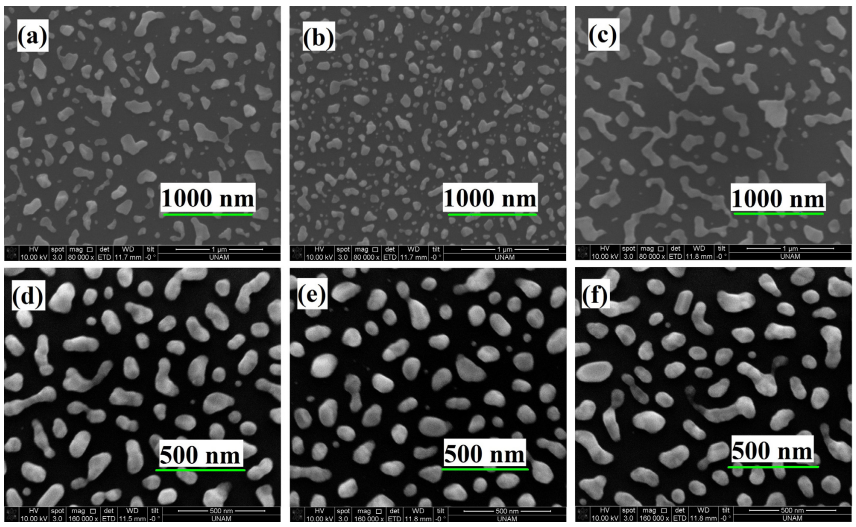

Fig. 1. SEM image of (a-c) gold nanoparticles after applying 600◦C heat for 20min with heating rate of 120 ◦C/min and cooling rate of 120 ◦C/min, heating rate of 120 ◦C/min and cooling rate of 600◦C/min and heating rate of 600 ◦C/min and cooling rate of 600◦C/min respectively, (d-f) silver nanoparticles after applying 500◦C heat for 20min with heating rate of 100 ◦C/min and cooling rate of 100 ◦C/min,, heating rate of 100 ◦C/min and cooling rate of 500◦C/min and heating rate of 500 ◦C/min and cooling rate of 500◦C/min respectively.

The optimized recipes are 600◦C and 500◦C for 20min to obtain gold and silver nanoparticles respectively [8]. Taking Figs. 1(a)-1(c) into account, it can be deduced that 5min (slower) heating and cooling results in somewhat uniform nanoparticles. Comparing all three gold images, it is clear that the most detrimental effect comes from 1min (faster) heating (Fig. 1(c)) in terms of achieving more uniform particles. We attribute this to short time available for the reconstruction of the metal surface during fast heating step. We believe the fast heating results in high local stress gradiants and rapid agglomeration from the defects between the metal and underlying dielectric sites. The fast cooling (Fig. 1(b)) on the other hand, applies sudden high strain which results in forming smaller residues from larger agglomerated nanoislands while slow cooling gives enough time for adjacent nanoislands to coalesce. There seems to be a trade-off between having small nanoisland residues and uniform particles. The same discussion also applies for silver nanoparticles (Figs. 1(d)-1(f)). However, our results show that silver is more unstable than gold which results in more uniform particles, with less needed temperatures. It is worth pointing out that the recipes are optimized with thin metals on aluminum oxide dielectric which will also be the main dielectric in our samples so that we can obtain the same distribution on MIM samples. Since the density of residues are not too high, we carried on with slow heating and fast cooling recipes in favor of the most uniformity possible.

2.2 MIM absorber

We study different stacks with main focus on changing the bottom metal of the MIM stack. The structure is illustrated in Fig. 2(a) for gold nanoisland case. We used transmittive quartz substrate to eliminate any contribution to absorption from substrate. The substrate was cleaned and 70nm bottom metal was thermally evaporated in 3-5 $\times$ 10^{-6} Torr in thermal evaporator. We apply this thickness to eradicate possibility of transmission of light from the bottom metal. Afterwards, 40nm dielectric was deposited using Cambridge Nanotech Savannah atomic layer deposition (ALD) system. Finally, as mentioned earlier, a 10nm deposition followed by RTA process was carried out. The reflection measurement setup is

Optics EXPRESS

also depicted in Fig. 2(b). A halogen illuminator is connected to microscope (Meiji Techno) and the reflection of light off the sample from one of the lenses of the microscope is fed to a Newport OSM2 spectrometer and the data is collected by interfacing the spectrometer with PC.

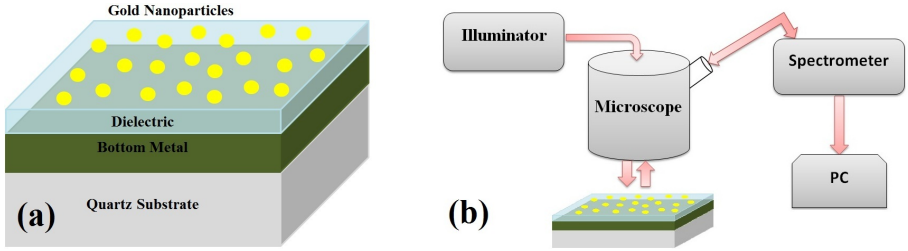

Fig. 2. (a) Schematic of the MIM structure, (b) Normal reflection measurement setup.

Figures 3(a) and 3(b) show the measured reflection percent for MIM structures with silver and gold nanoparticles respectively, while in each figure the bottom metal is selected as chromium, aluminum, gold and silver and 40nm aluminum oxide dielectric is kept constant. The reference mirror sample is taken to be thick aluminum for all experiments. All of the stacks generally exhibit reflection less than 20% in a vast proportion of the bands which justifies very high absorption; however, in order to investigate the potential of the stacks as PV devices, we need to delve into the contribution of different layers in absorption of the MIM stack, specially bottom metal, which is discussed in next section. The color tuning of the samples of Fig. 3(a) are represented in Fig. 4 which are visually congruent with the reflection results.

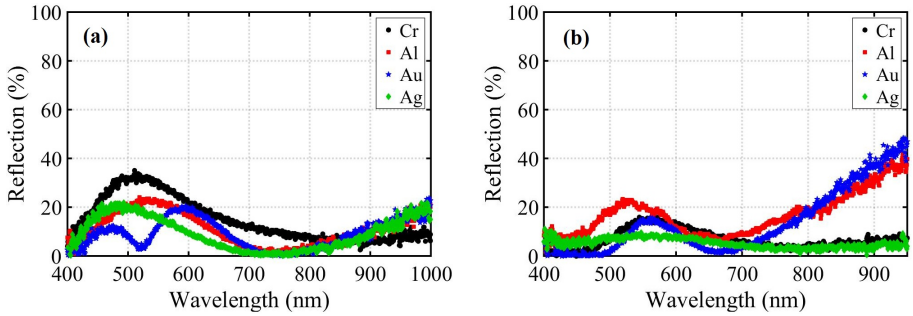

Fig. 3. Measured reflection for MIM stacks from bottom to top: 70nm different metals-40nm aluminum oxide- (a) silver nanoparticles and (b) gold nanoparticles.

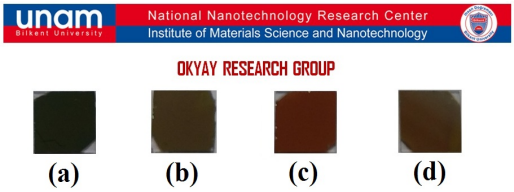

Fig. 4. Sample photos of MIM stacks from top to bottom comprised of silver nanoparticles-40nm aluminum oxide-70nm (a) chromium, (b)aluminum, (c)gold and (d) silver.

The result for comparison of 40nm-thick different dielectrics while we have aluminum as the bottom metal and silver nanoparticles on top is provided in Fig. 5. The spectral shapes exhibit a red shift as we increase the permittivity of the dielectric (I) in MIM stack. For the sample with titanium oxide for example, the second resonance falls out of our measurable range to more than 1000nm. The MIM stacks are optimized for maximum absorption using 40nm aluminum oxide as the insulator. Consequently, we observe higher reflection minima

Optics EXPRESS

(lower absorption peaks) for stacks with other dielectrics (TiO_2 and ZnO). Moreover, aluminum oxide is the least defective insulator compared to zinc oxide and titanium oxide and thus shows negligible loss which is quite desirable for a PV device.

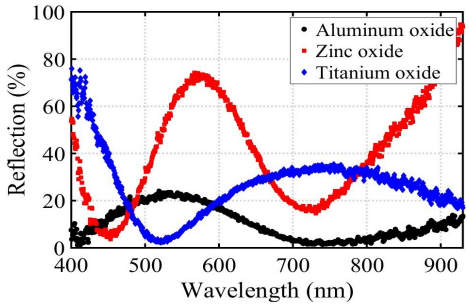

Fig. 5. Measured reflection for MIM stacks with silver nanoparticles on top and 70 nm aluminum as bottom metal and 40 nm of different dielectrics in between.

3. Simulation and discussion

3.1 MIM structures with silver nanoparticles

We will focus on contribution of different layers in the MIM stack to overall absorption which opens a window to the design and applications of MIM stacks. Simulations are carried out using Lumerical FDTD software all in 3D. The SEM images of nanoparticles are imported and set a height of 40nm calculated from the fill ratio of these particles. We have used Palik [13] model for chromium, aluminum and silver, and Johnson and Christy [14] model for gold. The n,k data for aluminum oxide has been sampled from elipsometry using Woollam VASE Ellipsometer. Figure 6 illustrates the reflection and absorption simulation results and the comparison of them to measured values. Due to the presence of a thick metal layer (70-nm-thick) there is no measureable transmission from the samples. Therefore, the experimental reflection is measured and absorption is calculated by the relation A = 1-R. It can be concluded from the simulations that we have a little blue-shift in our experimental results compared to simulations which can be related to tarnishing in silver nanoislands due to exposure to air. It should also be pinpointed that if we had highly ordered nanoislands of the same size and distribution using e-beam lithography method, we would have obtained taller and narrower absorption peaks in bottom metals (results not provided here). However, when we have a distribution of random nanoislands, we will achieve lower and broader peaks.

It is deduced from Fig. 6 that the MIM structure with silver bottom metal exhibits the highest overall absorption in the VIS-NIR region. For hot electron based MIMIM type devices, however, absorption in bottom metal is critical. MIM structure with chromium, results in the highest absorption in the bottom metal layer, although the overall absorption in all layers combined is slightly lower than that of MIM structure with silver bottom metal. To elucidate absorption phenomenon further, it can be noted from Fig. 6 that LSP modes exist that extend to a broad range of wavelengths when we use highly reflecting bottom metals (gold and silver). On the other hand, in metals with higher losses, we observe SP modes at higher wavelengths and LSP in lower wavelengths. Moreover, we apprehend that for NIR applications, chromium and aluminum bottom metals (Figs. 6(b) and 6(d) respectively) have higher absorption compared to the cases of gold and silver. This issue is the most crucial trade-off in designing absorbers. This can be traced back to the fact that chromium and aluminum exhibit higher loss in these bands due to inherent material properties. The structure with the highest absorption, chromium bottom metal, exhibits a broad absorption of up to 45 percent at 1600nm (inset of Fig. 6(b)).

Optics EXPRESS

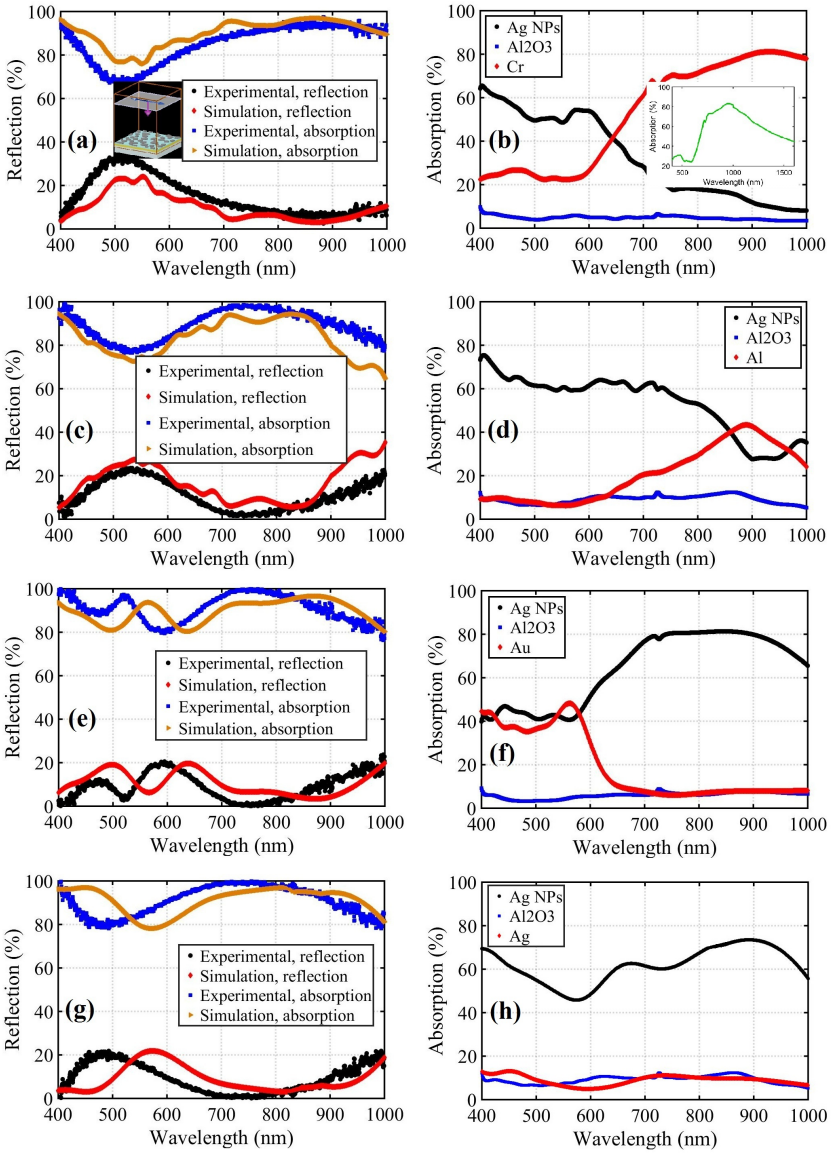

Fig. 6. Experimental and simulation results of reflection and absorption (left) and absorption in different layers (right) for silver nanoparticles-aluminum oxide- (a), (b) chromium, (c), (d) aluminum, (e), (f) gold and (g), (h) silver bottom metal. Inset of Fig. 6(a) represents the simulation region in lumerical FDTD and the inset of Fig. 6(b) shows the absorption in chromium up to 1600nm.

Figure 7 illustrates electric and magnetic field distribution for chromium and gold in a region randomly selected with two particles within the stack at the 400nm and 1000nm wavelengths. It can be inferred that the field patterns are roughly the same, while there is higher field intensity at 400nm for chromium bottom metal compared to the gold one which corresponds to higher reflection of chromium in the proximity of this wavelength. At 400nm, lower order plasmonic mode is excited and fields are mainly confined in silver nanoparticle-air interface (Figs. (7)a, (7)b, (8)a, and (8)b) while higher order modes exist at 1000nm confining light between the silver nanoparticle-aluminum oxide interface (Figs. 7(c), 7(d) and Fig. 8(c) and 8(d)). This gives rise to absorption probability in bottom metal. These

Optics EXPRESS

simulations are highly in accordance with the absorption behavior of chromium and gold in Fig. 6.

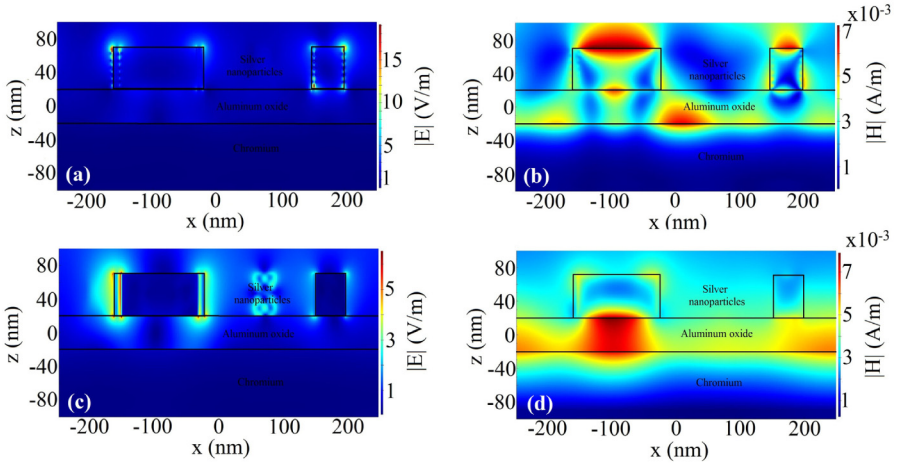

Fig. 7. Electric field and magnetic field magnitude simulation for silver nanoparticles-aluminum oxide-chromium structure at (a), (b) 400nm and (c), (d) 1000nm.

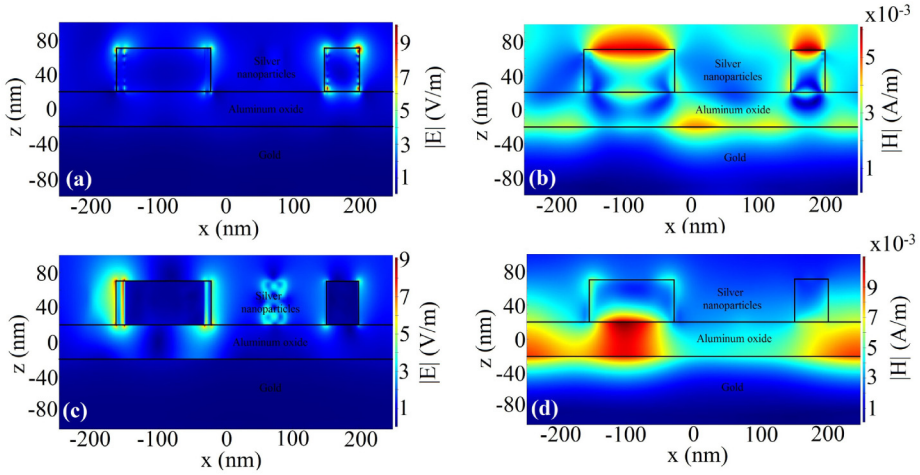

Fig. 8. Electric field and magnetic field magnitude simulation for silver nanoparticles-aluminum oxide-gold structure at (a), (b) 400nm and (c), (d) 1000nm.

Our results point out that MIM using Cr is more suitable than Au as a plasmonic absorber, somewhat contrary to intuition that Au is a more efficient plasmonic material at these wavelengths. We attribute this outcome to fundamental material models. A metal is considered a good absorber in a wavelength of interest, when it has low real permittivity (strong field penetration) and high complex permittivity (high absorption). The easiest way to analyze both components simultaneously is to consider electric loss tangent parameter of each metal which is defined as the ratio of the imaginary part of permittivity to its real part. Figure 9 puts forth the loss tangent magnitude versus wavelength for different bottom metals using the afore-mentioned permittivity data [13,14]. Loss tangent gives a more clear image of the plasma frequency of the metals and their absorption probability. As it is evident from Fig. 9(a), the plasma frequency of chromium and as a result, an extraordinarily high maximum of loss tangent magnitude happens at approximately 850nm which makes it the most suitable candidate for absorption in NIR region and this plays a crucial role in the high absorption of

Optics EXPRESS

chromium in MIM structure. Aluminum also does have a maximum which again is absorbing in NIR region. However, gold is more suitable for visible region as it can be elicited from Fig. 6(f) and 9(b).

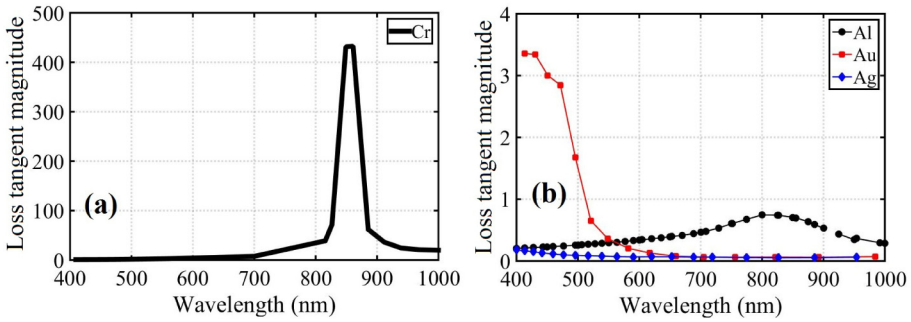

Fig. 9. Loss tangent magnitude versus wavelength for (a) chromium and (b) aluminum, gold and silver.

Moreover, gold and silver are both good scatterers (low loss) which makes sense to use them for nanoparticle layers due to low loss tangent. The absorption can be looked at from another viewpoint. Gold and silver have plasma frequency in ultraviolet (UV) region. Therefore, these two samples absorb within VIS which is close to UV. While in case of aluminum, the plasma frequency is deeper into the UV region therefore, we must seek the absorption in loss tangent characteristics. For chromium, plasma frequency happens at 850nm which makes it a prominent NIR absorber.

3.2 MIM structures with gold nanoparticles

Since the results for gold nanoparticles and the required discussion is analogous to the silver counterparts, we avoid redundancy. The only differentiating point is that since gold particles inherently are more random in shape and distribution, we have lower absorption peaks in bottom metals and broader spectral response due to the discussion cited before. It is a matter of preference though if we aim very broad response. The results for gold nanoisland samples are illustrated in Fig. 10. It is worth pointing out that there are some works which claim that Ag tarnishing can cause blue-shift, however, our structure is not identical to those reported. In addition, the random nature of the dewetting process, results in statistical variation in particle dimensions. In Ag and Au cases, the variations are not the same either. We try to capture the NPs sizes in simulations by importing from SEM images, however, there could still be slight difference since the SEM image has a limited view area. Therefore, we attribute the slight mismatch between the simulated and measured peaks (Fig. 10) to the statistical variation in particle sizes, in addition to potential contribution of tarnishing in the case of Ag particles.

Optics EXPRESS

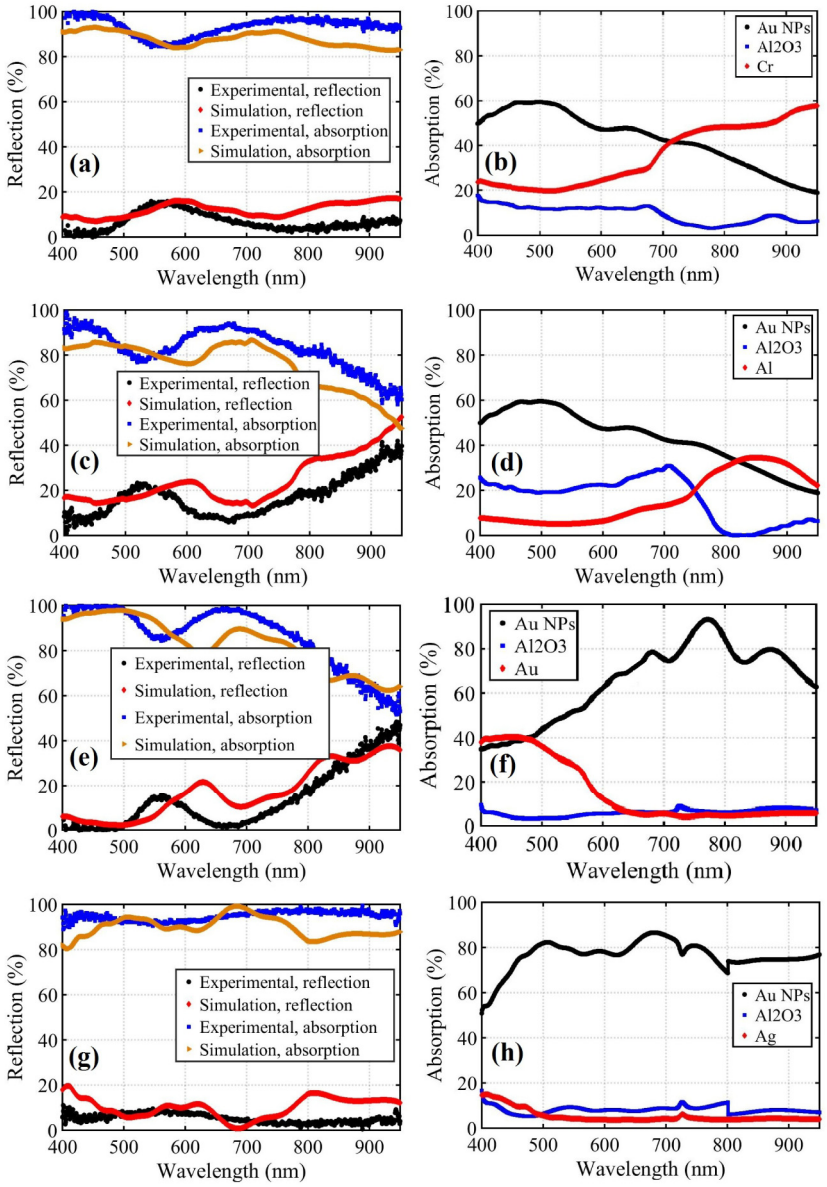

Fig. 10. Experimental and simulation results (left) and absorption in different layers (right) for gold nanoparticles-aluminum oxide- (a), (b) chromium, (c), (d) aluminum, (e), (f) gold and (g), (h) silver bottom metal.

4. Conclusion

We have investigated and proposed metal-insulator-metal stacks that are super absorbing in VIS-NIR region. Meanwhile, we introduce electric loss tangent magnitude to explain the counter-intuitive outcome that chromium is a better plasmonic absorber in the NIR. We use Lumerical FDTD to simulate and study the contribution of different parts of MIM stack in the overall absorption. The LSP modes along with SP modes at lower and higher wavelengths respectively, demonstrate the potential of these stacks in PV and photodetector devices. Gold bottom metal is appropriate for VIS region and chromium and aluminum are useful for NIR

Optics EXPRESS

applications. We also suggest chromium as a remarkable absorber bottom metal in both VIS and NIR regions due to its longer wavelength plasma frequency. Chromium has rarely been given the consideration it deserves in plasmonic absorbers; however, its higher resistivity might be controversial in efficiency for PV devices. Chromium in silver nanoparticles-aluminum oxide-chromium stack has a very high loss tangent and an absorption peak of 80 percent at 850nm, broad spectral shape ranging from 600nm to 1600nm if we set the absorption limit to no less than 50 percent. Once we resolve absorption, we can integrate the MIM stack on top of another insulator metal layer (tunneling bottom MIM) or simply a semiconductor (Schottky bottom MS) to collect the hot electrons or holes generated as a result of nonradiative plasmon decay in the absorbing bottom metal of MIM stacks.

Funding

Scientific and Technological Research Council of Turkey (TUBITAK) (112E052, 113M815); Turkish Academy of Sciences Distinguished Young Scientist Award (TUBA GEBIP) and BAGEP and FABED awards.